J Mol Model (2010) 16:1919–1929
DOI 10.1007/s00894-010-0679-7

ORIGINAL PAPER

Modeling the binding modes of stilbene analogs to cyclooxygenase-2: a molecular docking study

Souhila Bouaziz-Terrachet · Amel Toumi-Maouche · Boubekeur Maouche · Safia Taïri-Kellou

Received: 16 November 2009 / Accepted: 2 February 2010 / Published online: 17 March 2010

Abstract Stilbene analogs are a new class of anti-inflammatory compounds that effectively inhibit COX-2, which is the major target in the treatment of inflammation and pain. In this study, docking simulations were conducted using AutoDock 4 software that focused on the binding of this class of compounds to COX-2 protein. Our aim was to better understand the structural and chemical features responsible for the recognition mechanism of these compounds, and to explore their binding modes of interaction at the active site by comparing them with COX-2 co-crystallized with SC-558. The docking results allowed us to provide a plausible explanation for the different binding affinities observed experimentally. These results show that important conserved residues, in particular Arg513, Phe518, Trp387, Leu352, Leu531 and Arg120, could be essential for the binding of the ligands to COX-2 protein. The quality of the docking model was estimated based on the binding energies of the studied compounds. A good correlation was obtained between experimental logAr values and the predicted binding energies of the studied compounds.

Keywords Cyclooxygenase-2 · COX-2 · Molecular docking · AutoDock · Stilbenes · NSAIDs · Hydrophobic interactions

S. Bouaziz-Terrachet (✉) · A. Toumi-Maouche · B. Maouche · S. Taïri-Kellou
Laboratoire de Physico-Chimie Théorique et Chimie Informatique, Faculté de Chimie, USTHB B.P. 32, El Alia, Alger, Algeria
e-mail: souhilaterrachet@gmail.com

Introduction

Cyclooxygenase (COX), also known as prostaglandin endoperoxide H synthase (PGHS), catalyzes the conversion of arachidonic acid (AA), its natural substrate, to prostaglandin (PGs). This enzyme exists in two isoforms: PGHS-1 (or COX-1) and PGHS-2 (or COX-2), which perform the same enzymatic activities [1–3]. These enzymes are approximately 60% identical in terms of amino acid composition, and their catalytic regions are widely conserved [4–6]. Furthermore, the two active sites of these isoforms differ by only two amino acids, at positions 523 (Ile for COX-1 and Val for COX-2) and 513 (His for COX-1 and Arg for COX-2) [7]. COX-1 is homeostatic. It is expressed in many tissues, including the gastrointestinal tract, kidney, and platelets, whereas COX-2 is expressed at sites of inflammation, the hippocampus, female reproductive tissue, and in many cancers [8–11]. COX exhibits activity towards both cyclooxygenase and peroxidase. The first involves the conversion of AA to prostaglandin G_2 (PGG_2), while the second catalyzes the transformation of PGG_2 to prostaglandin H_2 (PGH_2), from which PGs, prostacyclin, and thromboxanes are derived.

Nonsteroidal anti-inflammatory drugs (NSAIDs) block the production of PGs by inhibiting both COX-1 and COX-2. Most of these drugs are associated with well-known side effects at the gastrointestinal level (mucosal damage, bleeding), and less frequently at the renal level. These drugs appear to produce at least some of their beneficial effects by inhibiting COX-2, and their deleterious side effects by inhibiting COX-1 [12]. Thus, selective inhibition of the induced enzyme, without affecting the homeostatic one, might avoid the side effects of currently available NSAIDs [12]. The differences between the active sites of COX-2 and COX-1 enzymes, which are described as hydrophobic channels, are the basis for the

design of COX-2 selective inhibitors (coxibs). Since coxibs (celecoxib, rofecoxib, valdecoxib, etoricoxib, lumeracoxib) fail to inhibit the constitutive COX-1 isoform, they have no adverse gastrointestinal effects. However, recent publications have suggested that some coxibs on the market have been associated with adverse cardiovascular side effects [13]. Thus, there is a need to design new compounds with optimum COX-1/COX-2 selectivity. Indeed, there are already several classes of compounds that are known to display selectivity towards COX-2, such as oxazoles, pyrazoles, pyrroles, and imidazoles [14–16]. The physiology and pathophysiology of COX continue to be topics of great interest [17–20]. A large number of research studies aimed at finding selective COX–2 inhibitors have been reported [21–27].

One of the research techniques employed to provide evidence of ligand binding sites on biological macromolecules is the computational docking method. This technique has been applied previously to the binding of several classes of inhibitors to the X-ray structure of PGHS [28–30]. In this context, we are interested in the ligand–protein binding—which is important not only as an essential molecular recognition process but also for the discovery of new COX-2 inhibitors—between a series of stilbene analogs and COX-2 protein.

In the present study, we use the AutoDock 4 program to perform the molecular docking of stilbene analogs with COX-2 protein. Our objective is to search for favorable binding modes and to gain insight into the interaction between these ligands and COX-2 protein. As the result, the correlation between the experimental binding affinities of the studied compounds and the AutoDock binding energies is investigated.

Materials and methods

Dataset preparation for AutoDock

The dataset used for this study contains 30 stilbene analogs, selected in order to define a manageable dataset characterized by adequate biological and structural diversity [31–34]. This dataset contains compounds that selectively inhibit COX-2, compounds that have binding affinity for both COX-1 and COX-2, and compounds that are inactive towards both enzymes. In order to simplify our analysis, we organized the 30 stilbene analogs into five groups according to the nature of their R_1, R_2, R_3, and R_4 substituents (Table 1). As their binding data were not obtained under the same experimental conditions, Table 1 provides the logarithms of the relative values, denoted Ar, which are calculated with respect to the same reference molecule: celecoxib, which is featured in all series arising from different sources [31–34]. The binding affinities, measured in vitro, are given in terms of IC_{50}, the drug concentration that inhibits 50% of the enzymatic activity of COX-2. Therefore, for each molecule, Ar = (IC_{50} of the molecule)/(IC_{50} of the celecoxib). The IC_{50} values of celecoxib according to different sources are listed in Table 2. The 2D structures of these compounds were drawn with standard geometric parameters using the molecular builder in ISIS/Draw as implemented in the ISIS 2.4 package [35], and they were converted to 3D format (.pdb) using ChemOffice 2003 [36], where geometrical optimization was performed with the MM2 method. The structures of the studied compounds, along with their IC_{50} and logAr values, are shown in Table 1 and Scheme 1.

Receptor preparation

The protein coordinates used in this study correspond to the X-ray structure of COX-2 bound with SC-558 (code 6cox determined at 2.80 Å resolution), which was downloaded from the Protein Data Bank [6]. The ligand and water molecules were removed, and all missing hydrogens were added. The active site radius was taken to be 8 Å from the centroid of the ligand, so that the amino acid residues (namely Arg120, Gln192, His90, Leu352, Leu359, Phe518, Trp387, Ser353, Tyr355, Tyr385, Arg513, Val523 and Val349) could be included. After assigning Gasteiger charges, nonpolar hydrogens were merged with their corresponding carbons. These preparations were done for each ligand using the Chimera [37] and AutoDockTools [38] packages.

Molecular docking using AutoDock

The thirty stilbene analogs were employed as the ligands while the docking process was performed. A two-step docking protocol was employed. In the first step, each ligand, placed in a random position, was flexibly docked into the active site using the default parameter means of the AutoDock 4 program [39]. This first-step approach served only to accommodate the different ligands into the binding site. The lowest-energy conformations obtained for each compound were then used as input for the second docking step.

In the second step, a grid map with 48×44×58 points around each of the modeled domains was used with a grid-point spacing of 0.375 Å. As a result, 30 grid parameters were created.

The docking procedure involved the AutoDock 4 program and its Lamarckian genetic algorithm (LGA), a new and promising hybrid search technique that implements an adaptive global optimizer with local search [40]. For all

Table 1 Structures (see also Scheme 1) of the thirty stilbene analogs studied, the original IC_{50} values (in μM) and logAr

Group	Molecule	R_1	R_2	R_3	R_4	IC_{50}	LogAr
1	C1	Ph	4-$NHSO_2Me$	H	n-C_6H_{13}	0.030	-0.368
	C2	Ph	4-$NHSO_2Me$	H	n-C_4H_9	0.320	0.660
	C3	Ph	4-$NHSO_2Me$	H	Et	1.800	1.410
	C4	Ph	4-$NHSO_2Me$	H	Me	33.100	2.675
	C5	Ph	4-$NHSO_2Me$	H	Cyclohexyl	>100	>3.155
2	C6	Ph	4-(N_3)	H	n-C_6H_{13}	0.110	0.196
	C7	Ph	4-(N_3)	H	n-C_4H_9	1.000	1.155
	C8	Ph	4-(N_3)	H	Et	0.280	0.602
3	C9	n-C_4H_9	4-SO_2Me	H	Ph	0.014	-0.609
	C10	n-C_4H_9	H	H	Ph	7.900	2.053
	C11	n-C_5H_{11}	4-SO_2Me	H	Ph	2.000	1.545
	C12	n-C_6H_{13}	4-SO_2Me	H	Ph	0.031	-0.264
	C13	Et	4-SO_2Me	H	Ph	1.250	1.341
	C14	Me	4-SO_2Me	H	Ph	0.630	1.043
	C15	H	4-SO_2Me	H	Ph	1.800	1.410
	C16	Et	4-SO_2Me	4-OH	Ph	1.900	1.434
4	C17	H	4-SO_2Me	H	CO_2H	3.000	1.632
	C18	H	4-SO_2Me	3-Br	CO_2H	0.310	0.646
	C19	H	4-SO_2Me	4-Br	CO_2H	3.600	1.711
	C20	H	4-SO_2Me	4-F	CO_2H	36.000	2.711
	C21	H	4-SO_2Me	4-OH	CO_2H	5.300	1.879
	C22	H	4-SO_2Me	4-OMe	CO_2H	1.900	1.434
	C23	H	4-SO_2Me	4-OAc	CO_2H	2.900	1.617
	C24	H	4-SO_2Me	4-NHAc	CO_2H	2.500	1.553
5	C25	H	4-SO_2Me	4-(2,4-F_2–C_6H_3)	CO_2H	0.320	0.660
	C26	H	4-SO_2Me	4-(4-i-PrO–C_6H_4)	CO_2H	0.320	0.660
	C27	H	4-SO_2Me	3-(2,4-F_2–C_6H_3)	CO_2H	>100	>3.155
	C28	H	4-SO_2Me	3-(4-i-PrO–C_6H_4)	CO_2H	>100	>3.155
	C29	H	4-SO_2Me	4-(4-MeO_2S–C_6H_4)	CO_2H	0.320	0.660
	C30	H	4-SO_2Me	3-(4-MeO_2S–C_6H_4)	CO_2H	2.100	1.477

dockings, 50 independent runs were used with step sizes of 0.01 Å for translations and 1.2° for orientations and torsions, 250,000 energy evaluations, a maximum number of generations of 27,000, an elitism value of 1, a mutation rate of 0.02, and a crossover rate of 0.8. The resulting positions were clustered according to the root mean square deviation (RMSD) criterion of 2.0 Å. Both Autogrid and AutoDock computations were performed on the Cygwin and Linux (Ubunto) platforms.

Table 2 Values of IC_{50} (μM) for the reference molecule, celecoxib, according to different sources

Reference	Molecule	IC_{50} celecoxib
[31]	C1–C8	0.070
[32]	C9, C11, C12, C13, C14	0.057
[33]	C10, C15, C16	0.070
[34]	C17–C30	0.070

Results and discussion

Selection of the most relevant conformation

Automated docking of the 30 studied compounds to the COX-2 active site resulted in several plausible docking orientations and conformations for each ligand. The resulting conformations were clustered into conformation

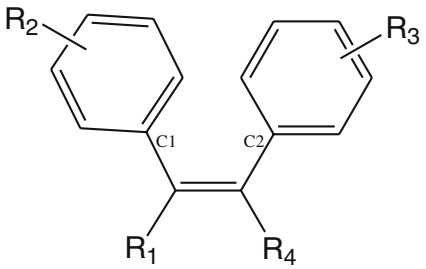

Scheme 1 General structure of the stilbene analogs studied in this work

families according to the RMSD criterion of lower than 2 Å. For most molecules there were one or two of the most densely populated clusters. These were sorted by energy (from lowest to highest), and their heights were proportional to the number of conformations in each cluster. The selection of the most relevant conformation among the conformations of the most populated cluster was done according to hydrogen bonding, binding energy and low RMSD. When the clusters had similar populations, we chose the conformations similar to those of other molecules.

Comparison between the X-ray structure and the docking structure

The structure of SC-558, extracted from the crystallographic complex 6cox, was used to set the optimal docking parameters for this study. The resulting conformation was close to the crystal structure (as shown in Fig. 1), since the RMSD between the two conformations was only 0.89 Å, which is quite satisfactory. Therefore, the studied compounds docked correctly to the COX-2 active site, with only a slightly different conformation from the crystal conformation.

Binding modes of the studied compounds

The docking results revealed that almost all of the compounds bind at the same binding site in the active site of the COX-2 protein (as determined experimentally). Molecular surface visualization shows that the active site of COX-2 is composed mostly of hydrophobic residues. There are three major pockets (S1, S2, S3) and one shallow pocket (S4) on the COX-2 active site (Figs. 2a and 2b).

Pocket S1: consists of the amino acid residues Ala516, Arg513, His90, Gln192 and the backbone of Phe518

Pocket S2: localized at the top of the channel, and consists of several hydrophobic amino acid residues: Tyr348, Tyt385, Phe518, Met522 and Trp387

Pocket S3: localized in the mouth of the active site, and is delimited by Leu359, Tyr355, Val116 and Arg120.

Pocket S4: shallow pocket localized in a hydrophobic area close to the hydrophobic pocket S2; it has little residues, including Leu534, Leu531 and Ile345.

Stilbene analogs can adopt two major conformations (A and B) in the COX-2 active site, which differ mainly in the 3D dispositions of the R_1, R_3 and R_4 groups and the olefinic C=C in the COX-2 active site. Comparison of the binding modes of the studied compounds with the X-ray structure of SC-558 shows that mode A is indeed most closely related to that observed in the crystallographic complex 6cox (Fig. 3).

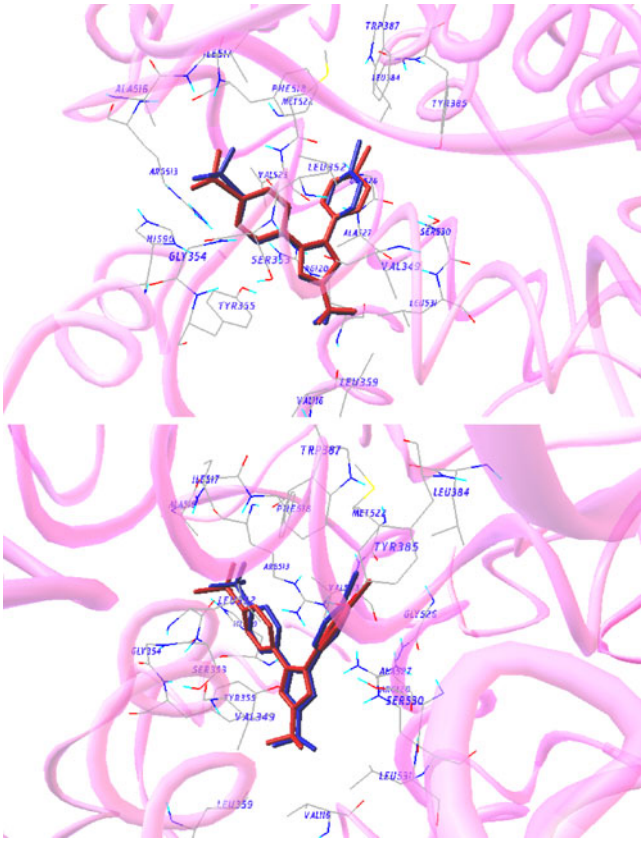

Fig. 1 Comparison between the X-ray structure and the docking structure for SC-558 (*blue*: docking, *red*: crystal structure). *Magenta ribbon* shows the protein backbone; only the amino acids within 5 Å of the docked ligand are presented. For the sake of clarity, two different viewing angles are provided

For both binding modes A and B, the automated docking suggests that the C-1 and C-2 phenyl groups are located in the vicinity of residues Val523, Phe518, Trp387 and Leu352, leading to π–π stabilizing interactions with the aromatic side chains of Phe518 and Trp387. Moreover, the backbone CO groups of Leu352 and Phe518 are linked to the ligand via hydrogen bonding with the polar group of the C-1 phenyl group (R_2 group).

In mode A, as shown in Fig. 4a, the olefinic C=C interacts with the hydrophobic residues Leu352 and Ala527. The residues Ser353 and Val523 are linked to the ligand via hydrophobic interactions with the C-1 phenyl group. The C-2 phenyl group is surrounded by Trp387, Tyr385, Phe518 and Val349, leading to hydrophobic interactions with these residues.

In mode B, as shown in Fig. 4b, the olefinic C=C interacts with Leu352 and Val523, resulting in favorable hydrophobic interactions. The C-1 phenyl group is surrounded by Phe518, Leu352 and Val523 and it interacts hydrophobically with

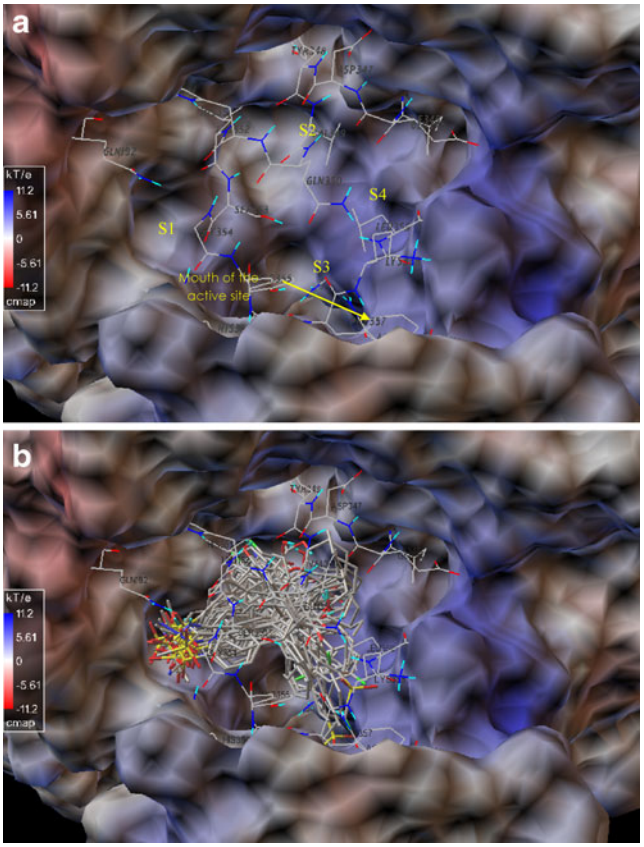

Fig. 2 **a** View of the surface of the binding site of COX-2. **b** View of the most favorable conformation of each compound (shown as a *stick*) docked into the COX-2 active site. The protein surface is colored according to electrostatic potential. Some residues are presented as lines to help visualize the COX-2 active site

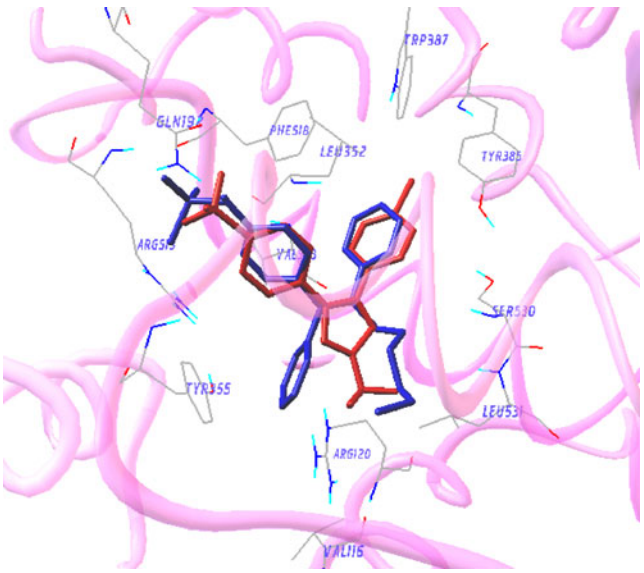

Fig. 3 Superposition of the most favorable binding mode of **C1** (*blue*) and the X-ray structure of SC-558 (*red*). *Magenta ribbon* shows the protein backbone

these residues. Leu531 and Ala527 are linked to the ligand via hydrophobic interactions with the C-2 phenyl group.

Representations of the selected binding modes of the studied compounds are given in Figs. 3, 4, 5 and 6. In all figures, for reasons of clarity, only the interacting residues of the active site are highlighted, while the hydrogen atoms are omitted. More detail regarding the binding modes is given in the following sections.

Docked conformations of group 1 compounds

Analysis of the data for this group, which have a $MeSO_2NH$ at the *para* position on the C-1 phenyl ring, leads to top conformations, all of which are in binding mode A. In this binding mode, the NH of the *p*-$MeSO_2NH$

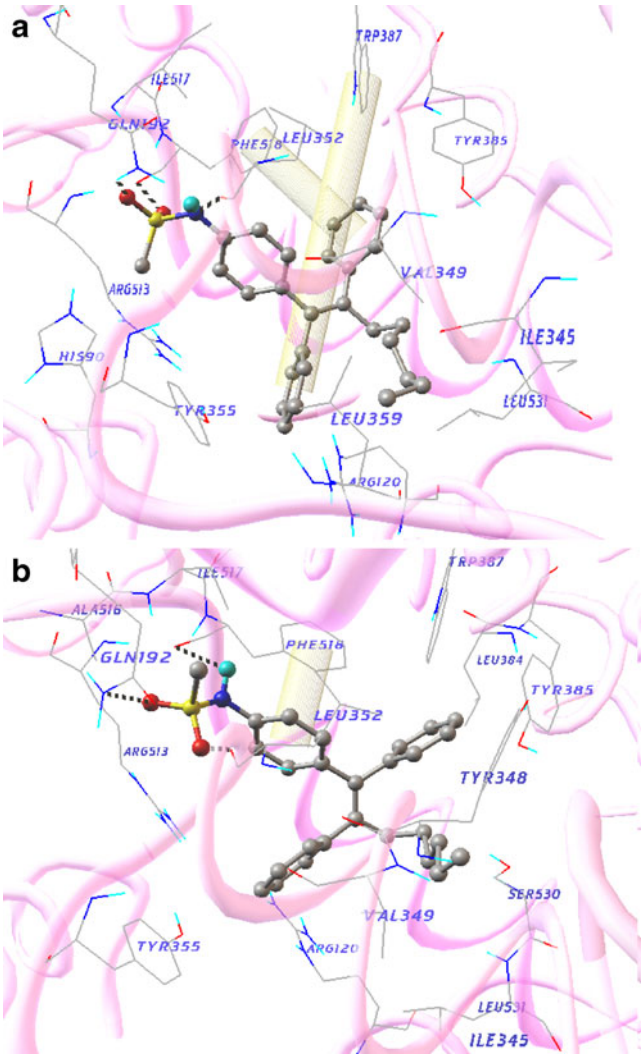

Fig. 4a–b View of the two possible binding modes for C1 obtained by molecular docking: **a** binding mode A; **b** binding mode B. Hydrogen bonds and π–π interactions are shown as *dotted black lines* and *transparent cylinders* for C1 in the COX-2 active site. *Magenta ribbon* shows the protein backbone

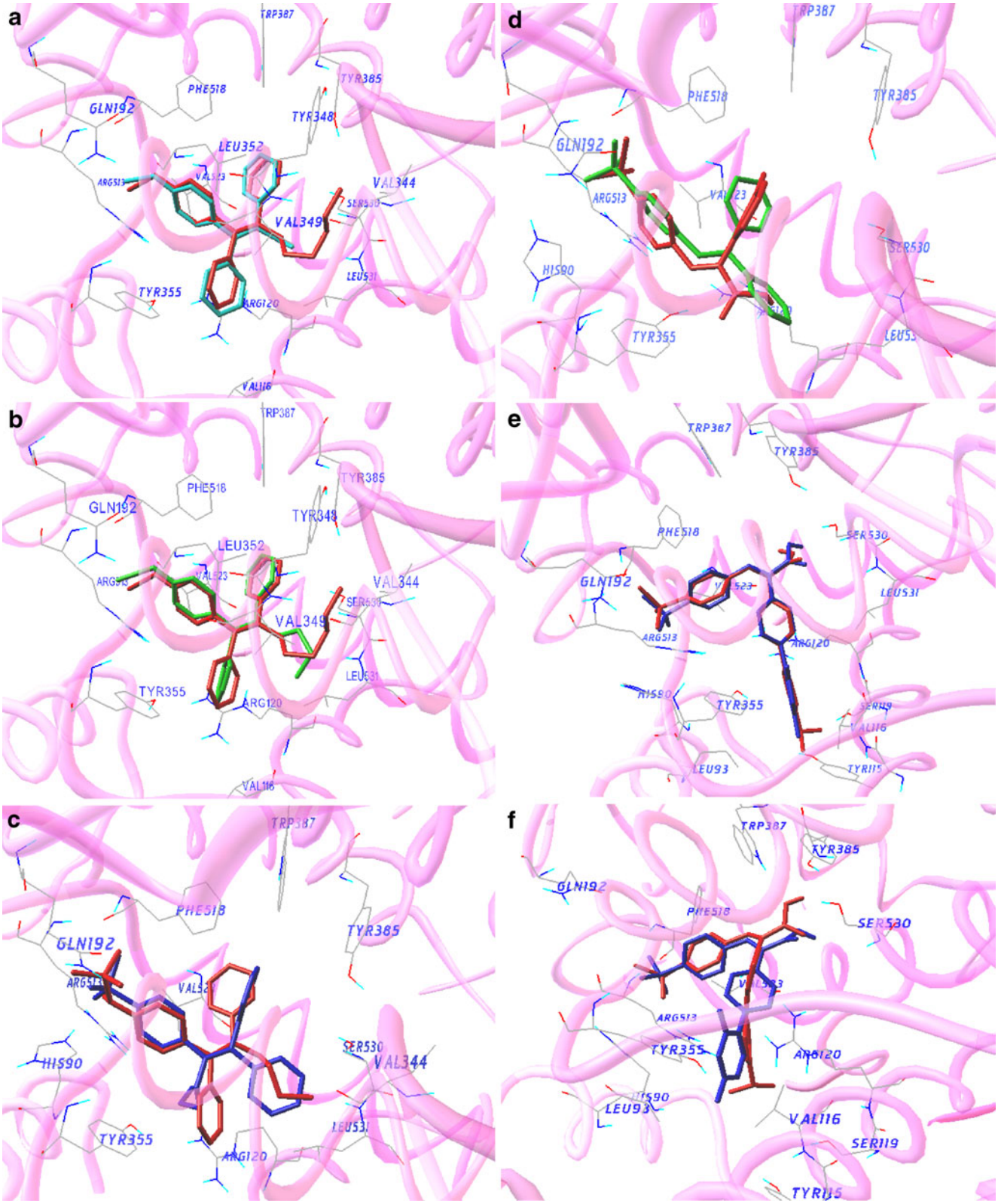

Fig. 5a–f Superpositions of selected conformations of compounds: **a C6** (*red*) and **C8** (*cyan*); **b C6** (*red*) and **C7** (*green*); **c C9** (*blue*) and **C2** (*red*); **d C18** (*red*) and **C15** (*green*); **e C25** (*blue*) and **C26** (*red*); **f C25** (*blue*) and **C29** (*red*). *Magenta ribbon* shows the protein backbone

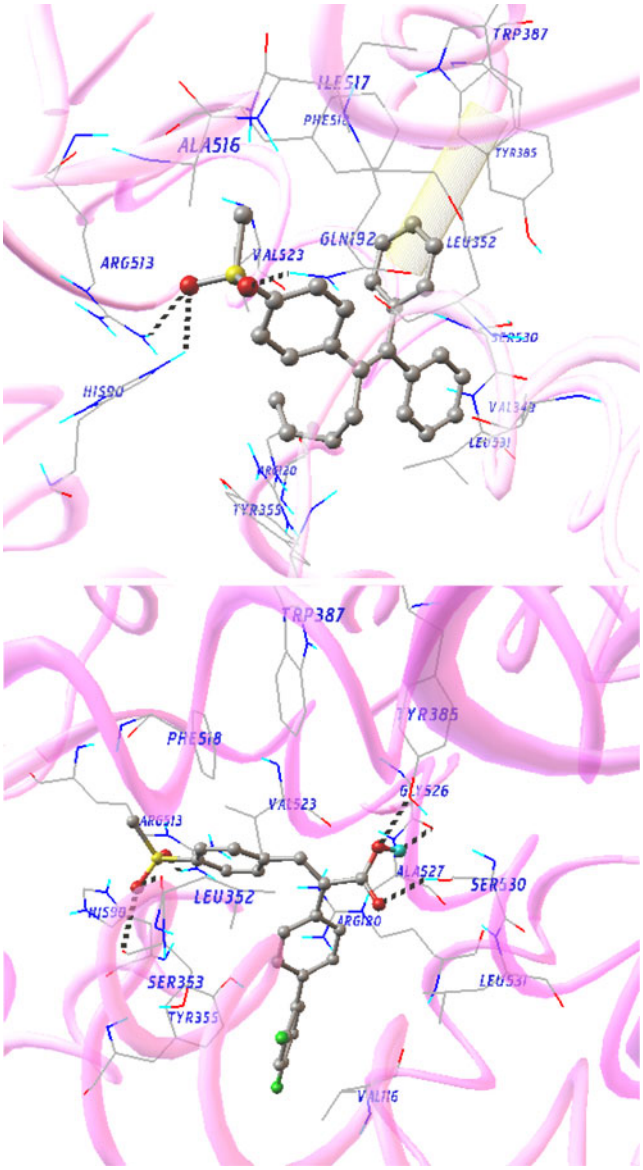

Fig. 6a–b Views of the most favorable binding modes for **a C9** and **b C25** obtained by molecular docking. Hydrogen bonds are shown as *dotted black lines* for **C9** and **C25** in the COX-2 active site. π–π interactions are shown as *transparent cylinders* for **C25** in the COX-2 active site. *Magenta ribbon* shows the protein backbone

group of compound **C1** is hydrogen bonded to the backbone CO of Leu352 (d=1.971 Å). One of the O atoms of *p*-$MeSO_2$ is hydrogen bonded to Gln192 (d=2.252 Å) and the NH backbone of Ile517 (d=3.159 Å), while the other O atom of *p*-$MeSO_2$ is hydrogen bonded to the backbone CO of Phe518 (d=2.870 Å). The C-2 n-hexyl group is close to Leu531, Val349, Ile345 and Leu359, as shown in Fig. 4a, resulting in aliphatic hydrophobic interactions with them. The C-1 phenyl ring, which is *cis* to the C-2 n-hexyl group, is oriented toward the mouth of the COX-2 binding site close to Tyr355 and Arg120, and is possibly involved with a cation–π interaction with the NH_2 group of Arg120 (d=4.023 Å). This interaction may have important COX-2 selectivity implications since it disrupts the salt bridge between Arg120 and Glu524 at the mouth of the COX-2 binding site [6, 41]. Figure 4b illustrates the hydrogen bond interactions of **C1** in its binding mode B at the COX-2 active site. This figure shows that the NH of **C1** forms one hydrogen bond with the backbone CO of Phe518, while the O atoms of *p*-$MeSO_2$ form two hydrogen bonds with Gln192 and the backbone CO of Leu352.

When the alkyl chain length was decreased, the inhibitory potency of COX-2 decreased, as indicated by **C2** (R_4 = n-butyl), **C3** (R_4 = ethyl) and **C4** (R_4 = methyl). The selected conformations for these compounds are characterized by an absence of interactions with Leu359, Leu531, Val349 and Ile345. It is worth noting that the alkyl chain length is an important influence on binding affinity. The cyclohexane ring in **C5** exerts more of a steric effect than the aliphatic groups in the pocket S4, and this pocket is required in new inhibitors.

Docked conformations of group 2 compounds

The replacement of $MeSO_2NH$ by its bioisostere, the linear dipolar *p*-azido group, as in compounds **C6**, **C7** and **C8**, leads to binding mode A. In the selected conformations of these compounds, the *p*-azido group is surrounded by Arg513, Val523 and His90. The distance between the terminal nitrogen of the *p*-N_3 group in these three conformations and the NH_2 of Arg513 is less than 5 Å. This result is in agreement with a model previously proposed [42] for another class of COX-2 inhibitors that have a *p*-azido group in which the N_3 group is involved in an electrostatic interaction with Arg513. The decrease in the binding potency of **C6** compared to that of **C1** can be explained by the lack of strong hydrogen bonds with Gln192 and the backbone CO of Phe518. The n-hexyl group of **C6** is pointed toward Val344, Tyr348 and Val349. On the other hand, in **C7** (R4 = n-butyl) and **C8** (R4 = ethyl), the lack of hydrophobic interactions with Val344 and Tyr348, as shown in Figs. 5a and 5b, could explain the moderate activities of these compounds observed experimentally.

Replacing the $MeSO_2NH$ or N_3 group by a $MeSO_2$ group, as in **C9**–**C30**, leads to the isopopulated binding modes A and B. Mode A is predominant in all compounds, except in those with a phenyl group at the *para* position on the C-2 phenyl group (**C26**–**C30**).

Docked conformations of group 3 compounds

Experimental binding affinity is strongly increased by converting the $MeSO_2NH$ of **C2** into $MeSO_2$ and interchanging the R_1 and R_4 groups, as in **C9**. Figure 5c

illustrates the comparative modes of docking of **C9** and **C2** into the COX-2 active site. However, the selected conformation for **C9**, the most potent COX-2 inhibitor among the selected compounds, is characterized by hydrogen bond interactions between the O atoms of *p*-$MeSO_2$ and Arg513 (d=3.005 Å), the NH of His90 (d=2.143 Å) and Gln192 (d=2.780 Å), as shown in Fig. 6a. Arg513 has been previously shown to be involved in a key hydrogen bond interaction with most selective COX-2 inhibitors [43]. Additionally, site-directed mutagenesis experiments identify this residue as being a critical determinant of COX-2 selectivity towards lipoamino acid N-arachidonylglycine (NAGly), which has been shown to suppress tonic inflammatory pain [44]. The C-1 n-butyl group is oriented towards Arg120 and Tyr355 and is involved in favorable hydrophobic interactions with these residues. The C-2 phenyl group which is *trans* to the C-1 *p*-$MeSO_2$ phenyl group is surrounded by the hydrophobic residues Val349 and Leu531. The distance between the center of this ring and Arg120 is 5.8 Å. The higher affinity of the $MeSO_2$, which is only capable of hydrogen bonding, of **C9** in comparison to the $NHSO_2Me$ of **C2** and the N_3 of **C7** may be attributed to the strong hydrogen bonding between an O atom of SO_2Me and the NH of His90. It is interesting to note that replacing the SO_2Me group by another group capable of hydrogen bonding (SO_2) and electrostatic interactions (N_3) with residues lining pocket S1 may increase the binding affinity of **C9**.

The decreased binding affinity of **C10** compared to that of **C9** may be due to the absence of the *p*-$MeSO_2$ group in the C-1 phenyl ring of **C10**. Comparing **C11** with **C9**, the n-pentyl group of **C11** has a greater steric effect on Arg120 than the n-butyl group does, and so this compound has a weaker affinity for COX-2. On the other hand, the last methyl of the *n*-hexyl group of **C12** is pointed toward Val116 and is involved in an aliphatic hydrophobic interaction with it. The lack of interactions between the R_4 group and Leu531 and Val116 may explain the low experimental activities of **C13** (R4 = ethyl), **C14** (R4 = methyl) and **C15** (R_4 = H) towards COX-2 protein. The insertion of the OH group at the *para* position on the C-2 phenyl group of **C13** decreases the enzyme-inhibiting potency, as seen in **C16**. However, the predicted bioactive conformation lacks the key interactions with residues Arg513 and Gln192. The lack of this hydrogen bond might explain the loss of activity observed experimentally, even if a hydrogen bond interaction between the backbone CO of Met522 and the OH group at the *para* position on the C-2 phenyl group is established.

Docked conformations of group 4 compounds

Replacing the unsubstituted C-2 phenyl group of **C15** by COOH, as in **C17**, leads to a decrease in the binding affinity. Previous studies have shown the importance of ionic interactions between the NSAID COOH group and Arg120 and its critical role in COX-1 inhibition [41, 45]. On the other hand, it is interesting to note that the COOH group undergoes both electrostatic and hydrogen-bonding interactions with polar amino acid residues [34]. Figure 5d illustrates the comparative docking modes of **C18** and **C15** at the COX-2 active site. However, in the selected conformation of **C18**, the distance between the OH group of COOH and the NH of Arg120 is 3.96 Å, and that between the carbonyl CO group of COOH and the NH_2 of Arg120 is 3.134 Å. Additionally, the bromo group at the *meta* position on the C-2 phenyl ring interacts hydrophobically with Met522 and Val523. The lack of these interactions when a bromo group is introduced at the *para* position, as in **C19**, decreases the binding affinity of this compound, even if an interaction between this group and Trp387 is established (d=3.84 Å).

Replacing the bromine in **C19** with fluorine, as in **C20**, leads to strong decrease in the experimental binding affinity. We speculate that the fluorine atom, which is less lipophilic than the bromine atom, exhibits decreased hydrophobic interaction in the pocket S2, which allows us to explain the decrease in the affinity of this compound to COX-2. This interaction is disfavored by the longer C=F bond compared to the C=Br bond (1.323 Å and 1.892 Å, respectively).

The introduction of an OH, OMe, OAc or NHAc group at the *para* position on the C-2 phenyl group of **C17**, as in compounds **C21**, **C22**, **C23** and **C24**, decreases the experimental binding affinity. In the selected conformation of each compound, the OH, OMe, OAc or NHAc group occupies the top hydrophobic pocket S2. The methyl of the *p*-OMe group of **C22** is an electron-donating group that increases the electron density of the oxygen atom so that it can form a hydrogen bond with Tyr385. As a result, the methyl of the *p*-OMe group of **C22** appears to be important for the inhibitory activity.

Docked conformations of group 5 compounds

The introduction of a phenyl group at the *para* or *meta* position on the C-2 phenyl group of **C17** leads to isopopulated binding modes A and B. The most populated binding mode corresponds to mode B. In this binding mode, the *p*-phenyl group of the C-2 phenyl ring is surrounded by Val349, Leu359, Val116, Tyr355 and Arg120.

The introduction of fluorine at the *para* and *meta* positions or an isopropyl group at the *para* position on the *p*-phenyl group in the C-2 phenyl ring, as in **C25** and **C26**, leads to the same experimental binding affinity. From Fig. 5e, we can see that the *p*-fluorine and *p*-isopropyl

groups are in the vicinity of Leu93, Ser119, Val116 and Tyr115. Figure 6b illustrates the hydrogen bond interactions of **C25** in its most favorable binding mode in the COX-2 active site. This figure shows that the O atoms of *p*-$MeSO_2$ form three hydrogen bonds with Arg513, Leu352 and Ser353, while COOH forms three hydrogen bonds with Ser530, Gly526 and Tyr385. This result is in agreement with mutagenesis experimental studies, which suggest that arachidonic acid and diclofenac bind to COX-2 in an inverted conformation with their carboxylate groups hydrogen bonded to Tyr385 and Ser530, leading to enzyme inactivity [46, 47]. Additionally, visualization of the selected binding conformation for **C25** shows a lack of π–π interactions with Trp387 and Phe518.

Moving the isopropylphenyl and difluorophenyl groups of **C25** and **C26**, respectively, to the *meta* position on the C-2 phenyl ring (as in **C27** and **C28**) led to inactive inhibitors of the COX-2 enzyme (IC_{50} > 100 μM). The strong decreases in the experimental binding affinities of these two compounds in comparison with those of **C25** and **C26** may be attributed to the unfavorable interaction between the *m*-phenyl group and Arg120 (Fig. 5f). However, the replacement of the isopropyl group in **C26** by $MeSO_2$, as in **C29**, leads to the same binding affinity; the main reason is that substitution at the *para* position of the *p*-phenyl group (R_3 group) does not influence the binding affinities of this series of compounds.

Moving the *p*-$MeSO_2$phenyl group on the C-2 phenyl ring of **C29** to the *meta* position on the C-2 phenyl ring (as in **C30**) leads to a hydrogen bonding interaction between the O atoms of *p*-$MeSO_2$ and the backbone CO of Phe357. The distance between the S atom of Met113 and an O atom of *p*-$MeSO_2$ in **C30** is 2.786 Å.

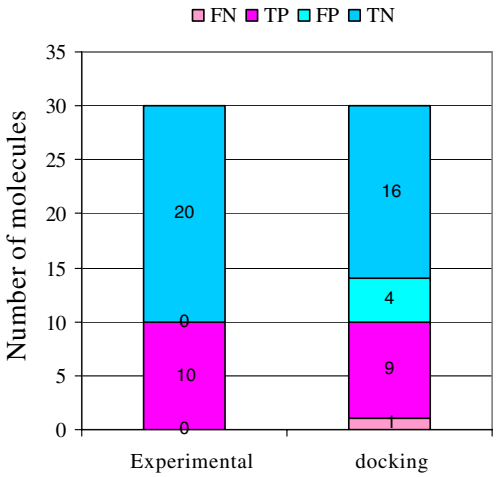

Fig. 7 Classification of the predictions made by the docking model for the thirty studied compounds

Table 3 Predicted binding modes, docking energies $\Delta G_{binding}$ (kcal mol^{-1}), and logAr values of the studied compounds

Molecule	Binding mode	$\Delta G_{binding}$	logAr
C1	Mode A	−15.80	−0.368
C 2	Mode A	−11.37	0.660
C 3	Mode A	−10.09	1.410
C 4	Mode A	−10.22	2.675
C5	Mode A	−8.42	>3.155
C6	Mode A	−11.92	0.196
C7	Mode A	−11.18	1.155
C8	Mode A	−11.36	0.602
C9	Mode A	−14.53	−0.609
C10	Mode A	−8.75	2.053
C11	Mode A	−11.32	1.545
C12	Mode A	−12.92	−0.264
C13	Mode A	−10.90	1.341
C14	Mode A	−11.40	1.043
C15	Mode A	−9.63	1.410
C16	Mode A	−9.91	1.434
C17	Mode A	−9.69	1.632
C18	Mode A	−12.76	0.646
C19	Mode A	−11.43	1.711
C20	Mode A	−7.49	2.711
C21	Mode A	−10.56	1.879
C22	Mode A	−10.73	1.434
C23	Mode A	−8.65	1.617
C24	Mode A	−11.46	1.553
C25	Mode B	−12.48	0.660
C26	Mode B	−10.43	0.660
C27	Mode B	−9.19	>3.155
C28	Mode B	−8.59	>3.155
C29	Mode B	−12.29	0.660
C30	Mode B	−10.95	1.477

Correlation between experimental affinities and predicted binding energies

The predicted binding energies ($\Delta G_{binding}$, obtained by the AutoDock program) of the studied compounds and the

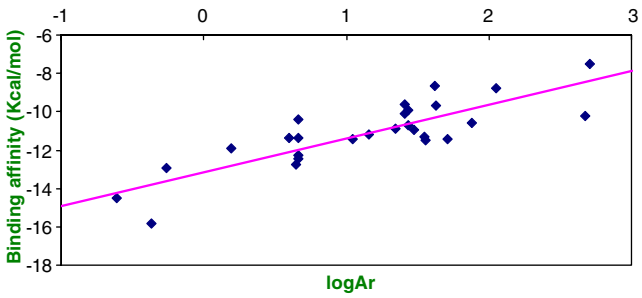

Fig. 8 Plot of the experimental logAr values versus the predicted binding energies $\Delta G_{binding}$ (kcal mol^{-1}) of the studied compounds (R=0.835)

corresponding experimental logAr values are listed in Table 3. The values in the table show that binding mode A is predominant compared to binding mode B. The logAr values of ligands can be grouped into two classes, active or inactive, based on whether the logAr value is less than 1 or more than 1, respectively. The docking energies of the inhibitors can be grouped into four classes: true positive (TP) or false positive (FP) when an inactive compound is predicted to be positive, and true negative (TN) or false negative (FN) when an active compound is predicted to be inactive. As a result, the active molecules are 90% correctly classified, while the inactive molecules are 80% correctly classified (Fig. 7). This indicates that there is a good correlation between the docking energies and the observed activities of the stilbene analogs.

The correlation between the calculated $\Delta G_{\text{binding}}$ values of the studied compounds and the experimental logAr values is plotted in Fig. 8, and a correlation coefficient R=0.835 was obtained. The straight line was obtained using the least squares method. Although this comparison represents the best correlation, considering the limitations of the available docking program and the fact that there are many unsolved areas, a value of 0.835 is not too discouraging. The ligand–receptor interaction is mediated by other factors, such as solvation effects and the flexibility and conformational changes of the receptor during binding with the ligand [48, 49]. Moreover, in the version of AutoDock used here, the receptor was treated as semi-flexible by selecting a few degrees of freedom to represent the protein flexibility [39]. The degrees of freedom chosen usually correspond to rotations around single bonds of some residues in the active site. However, the binding site still remains essentially rigid because the conformational changes of the protein are limited to a few terminal bonds.

Conclusions

In the present study, an automated docking procedure was applied in order to determine the optimal positions and orientations of thirty stilbene analogs in the binding site of COX-2. The quality of the docking model was estimated based on their binding energies. A good correlation (R=0.835) was observed between the experimental logAr values and the predicted binding energies of the studied compounds.

Docking results have allowed us to provide a plausible explanation of the different binding affinities observed by highlighting the most important interactions with COX-2 protein. These results are in agreement with previous site-directed mutagenesis studies on arachidonic acid and some COX-2 inhibitors [44, 46]. Most of the studied compounds have a very similar binding mode to that of the crystallographic complex 6cox. Two different binding modes, A and B, were predicted for this class of compounds within the active site of COX-2, which consists of three main pockets (S1, S2 and S3) and one shallow pocket (S4). Pocket S1 is composed mainly of lipophilic amino acids, while pockets S2, S3 and S4 are composed mostly of hydrophobic amino acids. It was found that the residues lining pocket S1, in particular His90, Gln192 and Arg513, may be essential for the binding of the ligand. Additionally, the backbone CO groups of Phe518 and Leu352 are predicted to be involved in hydrogen bonding interactions with the ligand. Some aromatic residues, in particular Phe518 and Trp387, may be essential for ligand recognition through π–π interactions. Arg120 was found to be essential for the ligand binding due to electrostatic interactions with the unsubstituted phenyl rings of the studied compounds.

This study shows that important conserved residues, in particular His90, Gln192, Arg513, Phe518, Leu352, Leu531, Trp387 and Arg120, could be specifically targeted in order to develop potential anti-inflammatory compounds. This study also opens up new perspectives for rational design in the development of new potential COX-2 inhibitors.

Acknowledgments Souhila Bouaziz-Terrachet wishes to warmly thank Lehtihet Abdelhalim El Amine and Redouane Terrachet of the EMP (Ecole Militaire Polytechnique) of Algeria for their help.

References

1. Smith WL, DeWitt DL, Garavito RM (2000) Annu Rev Biochem 69:145–182
2. Smith WL, DeWitt DL (1996) Adv Immunol 62:167–215
3. Marnett LJ, Rowlinson SW, Goodwin DC, Kalgutkar AS, Lanzo CA (1999) J Biol Chem 274(33):22903–22906
4. Picot D, Loll PJ, Garavito RM (1994) Nature 367:243–249
5. Luong C, Miller A, Barnett J, Chow J, Ramesha C, Browner MF (1996) Nat Struct Biol 3:927–933
6. Kurumbail RG, Stevens AM, Gierse JK, McDonald JJ, Stegeman RA, Pak JY, Gildehaus D, Miyashiro JM, Penning TD, Seibert K, Isakson PC, Stallings WC (1996) Nature 384:644–648
7. Zhang V, O'Sullivan M, Hussain H, Roswit WT, Holtzman MJ (1996) Biochem Biophys Res Commun 227:499–506
8. Sirois J, Richards JS (1993) J Biol Chem 268:21931–21938
9. Yamagata K, Andreasson KI, Kaufmann WE, Barnes CA, Worley PF (1993) Neuron 11:371–386
10. Seibert K, Zhang Y, Leahy K, Hauser S, Masferrer J, Perkins W, Lee L, Isakson P (1994) Proc Natl Acad Sci USA 91:12013–12017
11. Turini ME, DuBois RN (2002) Ann Rev Med 53:35–57
12. Singh R, Kumar R, Singh DP (2009) J Med Food 12(1):208–218
13. Prasit P, Wang Z, Brideau C, Chan CC, Charleson S, Cromlish W, Ethier D, Evans JF, Ford–Hutchinson AW, Gauthier JY, Gordon R, Guay J, Gresser M, Kargman S, Kennedy B, Leblanc Y, Léger S, Mancini J, O'Neill GP, Ouellet M, Percival MD, Perrier H, Riendeau D, Rodger I, Tagari P, Thérien M, Vickers P, Wong E, Xu LJ, Young RN, Zambouni R (1999) Bioorg Med Chem Lett 9:1773–1778
14. Li S, Zheng Y (2006) Int J Mol Sci 7:220–229

15. Biava M, Porretta GC, Cappelli A, Vomero S, Manetti F, Botta M, Sautebin L, Rossi A, Makovec F, Anzini M (2005) J Med Chem 48:3428–3432
16. Bosch J, Roca T, Catena JL, Llorens O, Pérez JJ, Lagunas C, Fernàndez AG, Miquel I, Fernàndez-Serrat A, Farrerons C (2000) Bioorg Med Chem Lett 10:1745–1748
17. FitzGerald GA (2004) N Engl J Med 351:1709–1911
18. Solomon DH, Schneeweiss S, Glynn RJ, Kiyota Y, Levin R, Mogun H, Avorn J (2004) Circulation 109:2068–2073
19. Finckh A, Aronson MD (2005) Ann Intern Med 142:212–214
20. Dogné JM, Supuran CT, Pratico D (2005) J Med Chem 48:2251–2257
21. Chavatte P, Yous S, Marot C, Baurin N, Lesieur D (2001) J Med Chem 44:3223–3230
22. Desiraju GR, Gopalkrishnan B, Jetti RK, Nagaraju A, Raveendra D, Sarma JA, Sobhia ME, Thilagavathi R (2002) J Med Chem 45:4847–4857
23. Liu H, Huang X, Shen J, Luo X, Li M, Xiong B, Chen G, Shen J, Yang Y, Jiang H, Chen K (2002) J Med Chem 45:4816–4827
24. Soliva R, Almansa C, Kalko SG, Luque FJ, Orozco M (2003) J Med Chem 46:1372–1382
25. Garg R, Kurup A, Mekapati SB, Hansch C (2003) Chem Rev 103:703–732
26. Murias M, Handler N, Erker T, Pleban K, Ecker G, Saiko P, Szekeres T, Jäger W (2004) Bioorg Med Chem 12:5571–5578
27. Baurin N, Mozziconacci JC, Arnoult E, Chavatte P, Marot C, Morin-Allory L (2004) J Chem Inf Comput Sci 44:276–285
28. Chen YC, Chen KT (2007) Acta Pharmacol Sin 12:2027–2032
29. Dilber SP, Dobric SLJ, Juranic ZD, Markovic BD, Vladimirov SM, Juranic IO (2008) Molecules 13:603–615
30. Ermondi G, Caron G, Lawrence R, Longo D (2004) J Comput Aided Mol Des 18:683–696
31. Uddin MJ, Praveen Rao PN, Knaus EE (2005) Bioorg Med Chem 13:417–424
32. Uddin MJ, Rao PN, Knaus EE (2004) Bioorg Med Chem Lett 14:1953–1956
33. Uddin MJ, Rao PN, Knaus EE (2004) Bioorg Med Chem 12:5929–5940
34. Moreau A, Chen QH, Praveen Rao PN, Knaus EE (2006) Bioorg Med Chem 14:7716–7727
35. MDL Information Systems (2002) ISIS/Draw 2.5. MDL Information Systems, San Leandro
36. Cambridge Scientific Computing (2003) ChemOffice Ultra. Cambridge Scientific Computing, Cambridge
37. Pettersen EF, Goddard TD, Huang CC, Couch GS, Greenblatt DM, Meng EC, Ferrin TE (2004) J Comput Chem 25(13):1605–1612
38. Sanner MF (1999) J Mol Graphics Mod 17:57–61
39. Morris Garrett M, Goodsell David S, Halliday Robert S, Huey R, Hart WE, Belew RK, Olson AJ (1998) J Comput Chem 19:1639–1662
40. Solis FJ, Wets RJB (1981) Math Operations Res 6:19–30
41. Greig GM, Francis DA, Falgueyret JP, Ouellet M, Percival MD, Roy P, Bayly C, Mancini JA, O'Neill GP (1997) Mol Pharmacol 52:829–838
42. Rao PN, Uddin MJ, Knaus EE (2004) J Med Chem 47:3972–3990
43. Zebardast T, Zarghi A, Daraie B, Hedayati M, Dadrass OG (2009) Bioorg Med Chem Lett 19:3162–3165
44. Kozak KR, Prusakiewicz JJ, Rowlinson SW, Schneider C, Marnett LJ (2001) J Biol Chem 276:30072–30077
45. Selinsky BS, Gupta K, Sharkey CT, Loll PJ (2001) Biochemistry 40:5172–5180
46. Rowlinson SW, Kiefer JR, Prusakiewicz JJ, Pawlitz JL, Kozak KR, Kalgutkar AS, Stallings WC, Kurumbail RG, Marnett LJ (2003) J Biol Chem 278:45763–45769
47. Kiefer JR, Pawlitz JL, Moreland KT, Stegeman RA, Hood WF, Gierse JK, Stevens AM, Goodwin DC, Rowlinson SW, Marnett LJ, Stallings WC, Kurumbail RG (2000) Nature 405:97–101
48. Teague SJ (2003) Nat Rev Drug Discov 2:527–541
49. Gunasekaran K, Nussinov R (2007) J Mol Biol 365:257–273